MATERIALS AND METHODS

Imaging techniques

The trimodality PET/CT-MR system consists of a full ring time-of-flight (TOF) 64-slice PET/CT (Discovery PET/CT 690 VCT, GE Healthcare, Waukesha, WI, USA) and a 3-Tesla MR (Discovery MR 750w, GE Healthcare), which are connected by a shuttle system. The detailed specifications of this system were described in previous studies (1-3). The potential misalignement of this system is insignificant, and does not bias clinical image reading (4). Software-based image co-registration was used as well.

Patients fasted at least 4 hours prior to being injected with a standardized dose of 350 MBq of FDG. Blood glucose concentration was measured before the FDG injection. According to our institutional guidelines, patients were referred to an endocrinologist and rescheduled if the blood glucose concentration was above 10 mmol/l. The total uptake time was set to 60 minutes. After 40 minutes, patients were transferred into the MR machine for the rest of the uptake time. All MR images were acquired during these 20 minutes (total MR acquisition time: 16 minutes). Then patients were transferred to the PET/CT machine, where acquisition started subsequently, at 60 min after the injection (total PET/CT acquisition time: 12 – 16 min. No intravenous contrast was given for CT or MR.

MR

Two radiofrequency coils in combination (GEM 16-element anterior array and GEM 40-element posterior array, GE Healthcare) were used for the MR acquisition. The MR protocol consisted of three pulse sequences.

Whole-body multi-section imaging was done with an axially acquired T1-weighted 3D dual-echo fast spoiled gradient echo sequence (Liver accelerated volume acquisition [LAVA]-Flex; GE Healthcare) and a coronal short TI inversion recovery (STIR) sequence without breath-hold. For

LAVA, two echoes were acquired sequentially within the same time of repetition (TR). Time to echo (TE) was set to fat/water opposed phase (OP) and in-phase (IP) in 3T, respectively. Water-only (WO) and fat-only (FO) images from the dual-echo acquisition were decomposed using an online two-point Dixon-based technique with correction algorithm (5). For the lung, a T2-weighted sequence with motion correction (periodically rotated overlapping parallel lines with enhanced reconstruction [Propeller], GE Healthcare) was acquired axially during free breathing, using respiratory triggering (6). The acquisition time is depending on the individual respiratory rate. Electrocardiographic triggering was not used. The total MR acquisition took approximately 16 minutes. The rationale for this rather short MR protocol was to keep the MR acquisition time equal to the PET acquisition time, so that this protocol could be implemented into a fully integrated PET/MR without impact on the total acquisition time compared to PET/CT.
Technical details are given in supplemental table 2 and have been published previously (1).

Surgery and non-surgical therapy

Subsequent thoracic surgery with curative intent was performed in 20 subjects and included mediastinal lymphadenectomy. Surgery for the primary tumor consisted mainly of lobectomy (18 subjects), while 3 subjects underwent pulmonary wedge resection (one of those together with lobectomy). Four patients underwent surgical resection of distant metastases (2 intrathoracic, 2 extrathoracic). Eleven of these 20 patients underwent subsequent adjuvant chemotherapy, and 2 patients underwent adjuvant mediastinal radiotherapy only.
Based on clinical results and imaging examinations, thoracic surgery was refrained from in the remaining 22 patients. Those received radiochemotherapy (12 subjects), chemotherapy only (7 subjects), or immunotherapy only (1 subject). Two patients died before the initiation of radiochemotherapy, one thereof died from the underlying oncological illness.

Image analysis

Anonymized image datasets were assessed in random order by two independent review boards of dually trained radiologists / nuclear medicine physicians with 7 – 12 years of experience in both MR and PET/CT interpretation. Readers were blinded to all patient data other than the suspicion of NSCLC. Tumor analysis criteria were lesion size, distance from main bronchus and carina, presence of distal atelectasis, nodular changes of pleura or pericardium, nodules in same or different lobe, infiltration of diaphragm, chest wall, mediastinum, esophagus, trachea, main bronchus, carina, heart, great vessels, spine (e.g. loss of fat planes, visible tumor extension into these structures etc.) on CT and MR, and uptake above background within lung or mediastinum, uptake of pleural effusion etc. on PET.

RESULTS

Histopathological results of study subjects are given in supplemental table 3. A complete pathological TNM staging was done in 20 subjects, and disease was classified as stage IA in 6 subjects, IB in 1, IIA in 4, IIB in 2, IIIA in 4, IIIB in 2, and IV in 1. Disease in the 22 subjects without complete pathological TNM staging was classified as stage IIIA in 3 subjects, stage IIIB in 8, and stage IV in 11.

T staging

Of the 4 subjects that were classified as correct but equivocal by PET/CT, 3 were classified correspondingly by PET/MR, while 1 subject was classified incorrectly. Of the 4 subjects classified incorrectly by PET/CT, 2 were also classified incorrectly by PET/MR, while 1 subject was classified as correct, and another one as correct but equivocal. In one of the latter two subjects, PET/CT underestimated the tumor size, while chest wall infiltration was missed in the other one.

N staging

In one patient, contralateral mediastinal lymph nodes were rated as inflammatory both by PET/CT and PET/MR, but contrast-enhanced CT and follow-up imaging confirmed lymph node metastases. In another patient, small ipsilateral mediastinal lymph nodes were interpreted as metastatic by both modalities, but contrast-enhanced CT, follow-up imaging and a review of the patient's history confirmed granulomatous disease. In one patient, PET/CT and PET/MR suspected ipsilateral hilar nodal metastases, but biopsy guided by endobronchial ultrasound was negative. In another patient, PET/CT suspected supraclavicular and ipsilateral mediastinal lymph node metastases, while biopsy confirmed only mediastinal nodal disease, as did PET/MR. PET/MR suspected the presence of a contralateral mediastinal lymph node metastasis in one patient, who turned out to be free of local nodal disease after surgery, which had also been

correctly identified by PET/CT. In one patient, PET/MR missed a small ipsilateral hilar lymph node metastasis that was proven by subsequent surgery, while PET/CT rated nodal disease as correct but equivocal. In another two patients PET/MR also missed a hilar lymph node metastasis, which was then identified by biopsy in one patient and by contrast-enhanced CT and follow-up imaging in the other patient, while PET/CT was correct in both patients.

M staging

The single subject that was classified as correct but equivocal by PET/CT, was classified correctly by PET/MR. This subject had a small amount of malignant pleural effusion (M1a), as verified by aspiration cytology. In one patient, PET/MR correctly identified contralateral intrapulmonary nodules, but missed a small sclerotic metastasis in the iliac bone (M1b instead of M1a), which was identified correctly by PET/CT. In the same patient, PET/CT misinterpreted focal muscle uptake as metastasis, which was rated as negative by PET/MR and confirmed as negative by contrast-enhanced CT, ultrasound and follow-up. This false positive PET/CT finding did not change the correct M staging in this individual, however. One patient with a perirenal metastasis was classified as correct but equivocal by PET/MR and as correct by PET/CT.
30 subjects were without distant metastases. Of the 24 thereof identified correctly by PET/CT, PET/MR identified 21. In one of the 3 inconsistent patients, PET/MR rated an FDG-avid consolidation in the contralateral lung as correct but equivocal for pneumonia rather than metastatic spread. In another patient, PET/MR findings were falsely positive for an adrenal metastasis, which was however eliminated by subsequent contrast-enhanced CT and MR imaging as well as follow-up. In the third patient, PET/MR mistook a traumatic rib fracture for a bone metastasis, as verified by contrast-enhanced CT, patient history and follow-up. Of the remaining 6 patients without distant metastasis, PET/CT findings (but not PET/MR) were falsely positive for an adrenal metastasis in one patient, which was ruled out by subsequent contrast-enhanced CT and MR imaging as well as follow-up. This patient underwent surgery and was

confirmed having stage pT1a pN0. In another patient, an adrenal adenoma was verified in the same way. This patient was rated as correct but equivocal by both PET/CT and PET/MR. In another patient, PET/CT but not PET/MR suspected a bone metastasis, which was however proven to be degenerative joint disease by contrast-enhanced MR and follow-up. In another patient, PET/MR suspected metastatic disease in an FDG-avid contralateral pulmonary nodule, while PET/CT rated this patient correct but equivocal. This nodule was proven to be inflammatory by histopathology. Two patients without evidence of malignant pleural effusion upon aspiration cytology were classified as correct but equivocal by PET/CT, while one was classified correctly and one incorrectly by PET/MR.

DISCUSSION

Resectability and T staging

Above all, the T stage of a tumor determinates its resectability (7, 8). The ability to differentiate between stages T3 and T4 is critical for any cross-sectional imaging modality, because T4 tumors are widely considered not resectable. T3 tumors are defined by their size (larger than 7cm), by the presence of main bronchus infiltration close to the carina (less than 2cm), by the presence of complete atelectasis behind the tumor, by growth into the chest wall, mediastinal pleura, diaphragm, and parietal layer of pericardium, as well as by the presence of metastases in the same lobe (9). The detection of infiltrative growth into the mediastinum and chest wall is facilitated by T2-weighted images without fat suppression and T1-weighted contrast-enhanced sequences (7). In our study we found no difference of PET/MR vs. PET/CT in the T staging. Adding contrast-enhanced breath-hold sequences for the chest region to a PET/MR protocol might be beneficial. Since most lung cancer patients referred for whole-body staging with PET recently underwent a chest CT, the by-trend inferior performance of PET/MR in the T staging might not play an important role in clinical practice.

N staging

The potential resectability of a tumor is also influenced by its N stage and M stage. In the presence of nodal metastases in the ipsilateral hilum or peribronchial area (N1), or in the ipsilateral mediastinum including the subcarinal space (N2), the tumor is still considered resectable. Nodes in the contralateral mediastinum or in the supraclavicular region, however, preclude curative surgery (10, 11).

M staging

The presence of distant metastasis may completely change the therapeutic approach in patients with potentially resectable disease based on the T stage and N stage. While some larger centers aim at resecting single small distant metastases in an attempt to let the patient qualify for curative surgery of the primary tumor, such an approach is precluded with multiple metastases being present. Although some reports by the group of Ohno state a similar accuracy of whole-body MR and PET/CT for M staging, PET/CT is the modality of choice for staging and re-staging lung cancer patients, which is reflected in international guidelines (10-15).

It is known that PET/CT misses lesions that are small or are located in organs with high background FDG activity, such as brain and liver, or might be falsely positive in the adrenal glands, which display variable physiologic FDG uptake (16-18). Hence, regionalized MR is recommended depending on the patient's symptoms and stage of disease (10, 11, 14, 15, 19). However, O'Dowd and colleagues estimated that 4.4% of 646 early-stage NSCLC patients who underwent surgery with curative intent, actually had occult brain metastases that would have been detected if MR were part of the initial staging (20). Even without specific organ protocols, PET/MR supposedly has a higher yield of distant metastases in asymptomatic patients than PET/CT, not only because of better anatomical detail, but also owing to tissue decomposition

properties of Dixon-type pulse sequences that are a prerequisite for MR-based AC in the body (21).

While there is a higher diagnostic confidence in *high-resolution* MR for the detection of bone metastases, whole-body MR and PET/CT are widely considered equal (22, 23). All liver and adrenal gland metastases in our cohort were detected by both modalities, while none of our patients had brain metastases. It was stated that contrast-enhanced PET/CT is equal to brain MR for detecting intracranial metastases (16). Our study used no i.v. contrast medium. It is well recognized that the brain is the “blind spot” of PET/CT in NSCLC, and therefore a brain MR is recommended to rule out brain metastases in stages IB and higher (19). Complementing a whole-body PET/MR in NSCLC with a contrast-enhanced short brain MR protocol of less than 15 minutes after the PET/MR should be able to deal with the issue of brain metastases readily.

REFERENCES

1. Huellner MW, Appenzeller P, Kuhn FP, Husmann L, Pietsch CM, Burger IA, et al. Whole-body nonenhanced PET/MR versus PET/CT in the staging and restaging of cancers: preliminary observations. Radiology. 2014;273(3):859-69.
2. Kuhn FP, Hullner M, Mader CE, Kastrinidis N, Huber GF, von Schulthess GK, et al. Contrast-enhanced PET/MR imaging versus contrast-enhanced PET/CT in head and neck cancer: how much MR information is needed? Journal of nuclear medicine : official publication, Society of Nuclear Medicine. 2014;55(4):551-8.
3. Appenzeller P, Mader C, Huellner MW, Schmidt D, Schmid D, Boss A, et al. PET/CT versus body coil PET/MRI: how low can you go? Insights into imaging. 2013;4(4):481-90.
4. Samarin A, Kuhn FP, Brandsberg F, von Schulthess G, Burger IA. Image registration accuracy of an in-house developed patient transport system for PET/CT+MR and SPECT+CT imaging. Nucl Med Commun. 2015;36(2):194-200.
5. Ma J. Breath-hold water and fat imaging using a dual-echo two-point Dixon technique with an efficient and robust phase-correction algorithm. Magn Reson Med. 2004;52(2):415-9.
6. Pipe JG. Motion correction with PROPELLER MRI: application to head motion and free-breathing cardiac imaging. Magn Reson Med. 1999;42(5):963-9.
7. Ohno Y, Adachi S, Motoyama A, Kusumoto M, Hatabu H, Sugimura K, et al. Multiphase ECG-triggered 3D contrast-enhanced MR angiography: utility for evaluation of hilar and mediastinal invasion of bronchogenic carcinoma. Journal of magnetic resonance imaging : JMRI. 2001;13(2):215-24.
8. Hochhegger B, Marchiori E, Sedlaczek O, Irion K, Heussel CP, Ley S, et al. MRI in lung cancer: a pictorial essay. The British journal of radiology. 2011;84(1003):661-8.

9. Edge SB, Compton CC. The American Joint Committee on Cancer: the 7th edition of the AJCC cancer staging manual and the future of TNM. Annals of surgical oncology. 2010;17(6):1471-4.

10. De Leyn P, Dooms C, Kuzdzal J, Lardinois D, Passlick B, Rami-Porta R, et al. Revised ESTS guidelines for preoperative mediastinal lymph node staging for non-small-cell lung cancer. European journal of cardio-thoracic surgery : official journal of the European Association for Cardio-thoracic Surgery. 2014;45(5):787-98.

11. Vansteenkiste J, Crino L, Dooms C, Douillard JY, Faivre-Finn C, Lim E, et al. 2nd ESMO Consensus Conference on Lung Cancer: early-stage non-small-cell lung cancer consensus on diagnosis, treatment and follow-up. Annals of oncology : official journal of the European Society for Medical Oncology / ESMO. 2014;25(8):1462-74.

12. Ohno Y, Koyama H, Nogami M, Takenaka D, Yoshikawa T, Yoshimura M, et al. STIR turbo SE MR imaging vs. coregistered FDG-PET/CT: quantitative and qualitative assessment of N-stage in non-small-cell lung cancer patients. Journal of magnetic resonance imaging : JMRI. 2007;26(4):1071-80.

13. Ohno Y, Koyama H, Onishi Y, Takenaka D, Nogami M, Yoshikawa T, et al. Non-small cell lung cancer: whole-body MR examination for M-stage assessment--utility for whole-body diffusion-weighted imaging compared with integrated FDG PET/CT. Radiology. 2008;248(2):643-54.

14. Silvestri GA, Gonzalez AV, Jantz MA, Margolis ML, Gould MK, Tanoue LT, et al. Methods for staging non-small cell lung cancer: Diagnosis and management of lung cancer, 3rd ed: American College of Chest Physicians evidence-based clinical practice guidelines. Chest. 2013;143(5 Suppl):e211S-50S.

15. Vansteenkiste J, De Ruysscher D, Eberhardt WE, Lim E, Senan S, Felip E, et al. Early and locally advanced non-small-cell lung cancer (NSCLC): ESMO Clinical Practice

Guidelines for diagnosis, treatment and follow-up. Annals of oncology : official journal of the European Society for Medical Oncology / ESMO. 2013;24 Suppl 6:vi89-98.

16. Hendriks LE, Bootsma GP, de Ruysscher DK, Scheppers NA, Hofman PA, Brans BT, et al. Screening for brain metastases in patients with stage III non-small cell lung cancer: Is there additive value of magnetic resonance imaging above a contrast-enhanced computed tomography of the brain? Lung cancer. 2013;80(3):293-7.
17. Lee HY, Lee KS, Kim BT, Cho YS, Lee EJ, Yi CA, et al. Diagnostic efficacy of PET/CT plus brain MR imaging for detection of extrathoracic metastases in patients with lung adenocarcinoma. Journal of Korean medical science. 2009;24(6):1132-8.
18. Schmidt GP, Baur-Melnyk A, Herzog P, Schmid R, Tiling R, Schmidt M, et al. High-resolution whole-body magnetic resonance image tumor staging with the use of parallel imaging versus dual-modality positron emission tomography-computed tomography: experience on a 32-channel system. Investigative radiology. 2005;40(12):743-53.
19. Ettinger DS, Wood DE, Akerley W, Bazhenova LA, Borghaei H, Camidge DR, et al. Non-small cell lung cancer, version 1.2015. Journal of the National Comprehensive Cancer Network : JNCCN. 2014;12(12):1738-61.
20. O'Dowd EL, Kumaran M, Anwar S, Palomo B, Baldwin DR. Brain metastases following radical surgical treatment of non-small cell lung cancer: is preoperative brain imaging important? Lung cancer. 2014;86(2):185-9.
21. Yi CA, Shin KM, Lee KS, Kim BT, Kim H, Kwon OJ, et al. Non-small cell lung cancer staging: efficacy comparison of integrated PET/CT versus 3.0-T whole-body MR imaging. Radiology. 2008;248(2):632-42.
22. Takenaka D, Ohno Y, Matsumoto K, Aoyama N, Onishi Y, Koyama H, et al. Detection of bone metastases in non-small cell lung cancer patients: comparison of whole-body diffusion-weighted imaging (DWI), whole-body MR imaging without and with DWI, whole-

body FDG-PET/CT, and bone scintigraphy. Journal of magnetic resonance imaging : JMRI. 2009;30(2):298-308.

23. Schmidt GP, Reiser MF, Baur-Melnyk A. Whole-body MRI for the staging and follow-up of patients with metastasis. European journal of radiology. 2009;70(3):393-400.

Supplemental Table 1

Acquisition parameters for PET/CT imaging

Parameter	
CT	
Tube voltage	120 kV (peak)
Reference tube current	12.35 mA / slice
Automated dose modulation range	15 – 80 mAs / slice
Collimation	64 x 0.625 mm
Pitch	0.948:1
Rotation time	0.5 s
Rotation speed	39.37 mm / rotation
Coverage speed	78.75 mm/s
FOV	50 cm
Noise index	20%
Reconstruction algorithm	Iterative (Adaptive Statistical Iterative Reconstruction (ASIR), GE Healthcare)
Soft- tissue images (non-overlapping)	
Kernel	Medium smooth convolution
Window center / width	40 / 400 HU
Slice thickness	1.25 mm
Isotropic pixel size	0.625 mm
Matrix	512 x 512 pixels
FOV	50 cm
Lung window images (non-overlapping)	
Kernel	Sharp convolution
Window center / width	-600 / 1200 HU
Slice thickness	1.25 mm
Isotropic pixel size	0.625 mm
Matrix	512 x 512 pixels
FOV	30 – 35 cm, depending on chest size
PET (3D mode)	
Scan duration	2 min / bed position
Bed positions	Max. 8 / scan, depending on patient size
Axial FOV	153 mm
Emission data correction	Randoms, dead time, scatter, attenuation
Attenuation-corrected images	
Reconstruction algorithm	Iterative (3D TOF OSEM: VUE Point FX, GE Healthcare)
Reconstruction parameters	3 iterations, 18 subsets
Matrix size	256 x 256 pixels

Note. – FOV: Field of view, HU: Hounsfield unit, OSEM: Ordered subset estimation maximization, PET/CT: Positron emission tomography / computed tomography, TOF: Time of flight.

Supplemental Table 2

Acquisition parameters for MR imaging

Parameter	LAVA	STIR	PROPELLER
TR / TE [ms]	4.3 / 1.3 (OP), 2.6 (IP)	2000 / 42	9321 / 122
Flip angle	12°	N/A	N/A
Partial Fourier	0.9%	N/A	N/A
TI [ms]	N/A	160	N/A
Parallel imaging acceleration factor	2	2	3
Slice thickness [mm]	4.0	6	4.5
FOV [cm]	50	50	40
Acquisition matrix	288 x 224 pixels	384 x 224 pixels	288 x 288 pixels
Receiver bandwidth [kHz]	142.86	100	62.5
Acquisition time per body section [s]	18	123	N/A
Body sections per patient	4	3	1
Total acquisition time [min]	ca. 3	ca. 8	ca. 5
Coverage	Whole body	Whole body	Chest, upper abdomen

Note. – FOV: Field of view, IP: In phase, LAVA: Liver acquisition with volume acquisition, N/A: Not applicable, OP: Opposed phase, PROPELLER: Periodically rotated overlapping parallel lines with enhanced reconstruction, STIR: Short TI inversion recovery, TE: Time to echo, TI: Inversion time, TR: Time of repetition.

Supplemental Table 3

Characteristics of study subjects

Parameter	Count
Study subjects	
Number	52
Gender	
Female	16 (31%)
Male	36 (69%)
Age (median, range) [years]	65 (31 – 85)
Tumor histology	
NSCLC	42 (81%)
Adenocarcinoma	30 (58%)
Squamous cell carcinoma	10 (19%)
Large-cell carcinoma	2 (4%)
Other	10 (19%)
Mutational status of NSCLC	
EGFR	Mutation: 0 (0%), wild type: 8 (19%), n/a: 34 (81%)
EML4-ALK fusion	Positive: 0 (0%), negative: 7 (17%), n/a: 35 (83%)
KRAS	N/a: 42 (100%)
TNM classification of NSCLC (7^{th} edition)	
T stage	
1a	9 (21%)
1b	4 (10%)
2a	7 (17%)
2b	5 (12%)
3	7 (17%)
4	10 (24%)
N stage	
0	10 (24%)
1	6 (14%)
2	11 (26%)
3	15 (36%)
M stage	
0	30 (71%)
1a	2 (5%)
1b	10 (24%)

Note. – All subjects underwent histopathological assessment of their primary tumor. Twenty (48%) of the subjects with NSCLC underwent surgery including lymphadenectomy. Two patients underwent assessment of their nodal status by biopsy without surgery. In these patients, pathological T stage (n = 20) and N stage (n = 22) were available. In the remaining subjects, clinical T stage (n = 22) and N stage (n = 20) served as standard of reference. The M stage was determined clinically in all subjects. ALK: Anaplastic lymphoma kinase, EGFR: Epidermal growth factor receptor, EML4: Echinoderm microtubule-associated protein-like 4, KRAS: Kirsten rat sarcoma viral oncogene homolog, NSCLC: Non-small cell lung cancer, TNM: Tumor – node – metastasis.

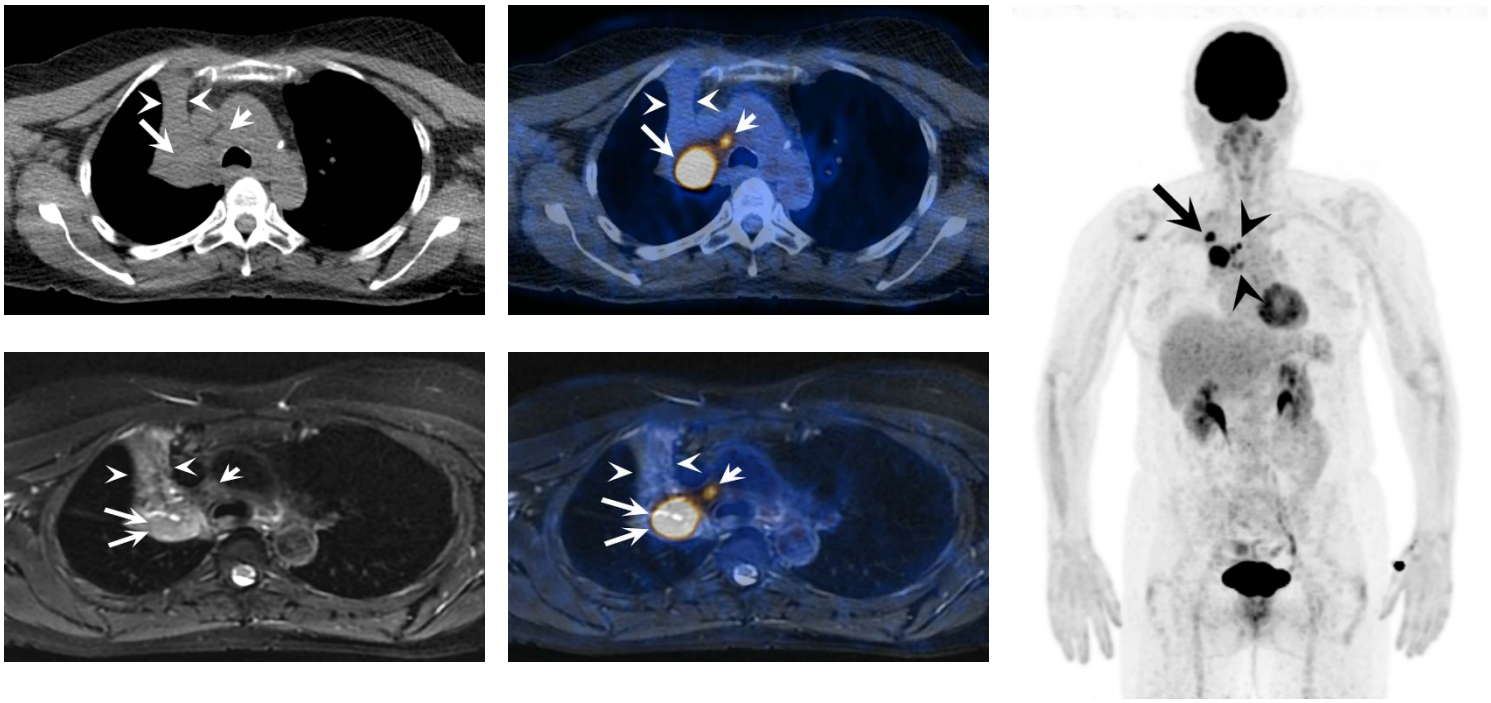

Supplemental Figure 1: Sixty-three year old woman with lung cancer in the right upper lobe stage T3 N2 M0. Axial CT image in mediastinal window display (a) shows a lung mass (arrow) in the central region on the right side, which is not well seen, and a post-obstructive atelectasis of the entire lobe (arrow heads). An ipsilateral mediastinal lymph node metastasis is seen as well (short arrow). Axial co-registered PET/CT image (b) confirms a highly FDG-avid central tumor (arrow) and the mediastinal lymph node metastasis (short arrow), while the atelectatic segments are not pathologically FDG-avid (arrow heads). Coronal PET MIP image (c) confirms the presence of multiple ipsilateral mediastinal lymph node metastases (arrow heads) and of an FDG-avid nodule in the same lobe (arrow) within atelectatic lung, as well as the absence of distant metastases. Axial Propeller image (TR 9321 ms, TE 122 ms) (d) and co-registered PET/Propeller image (e) display the primary tumor (arrows) with more anatomical detail and enable a morphological differentiation from the atelectatic lung (arrow heads). The lymph node metastasis (short arrow) is seen as well. Bronchoscopy confirmed infiltration of the main bronchus, which was rated as correct but equivocal by PET/MR.

ACRONYMS AND ABBREVIATIONS

3D	Three-dimensional
AC	Attenuation correction
ALK	Anaplastic lymphoma kinase
AUC	Area under the curve
CI	Confidence interval
CT	Computed tomography
EGFR	Epidermal growth factor receptor
EML4	Echinoderm microtubule-associated protein-like 4
FDG	^{18}F-fluoro-2-deoxy-*D*-glucose
FO	Fat-only
FOV	Field of view
GRE	Gradient-recalled echo
HU	Hounsfield unit
IP	In-phase
KRAS	Kirsten rat sarcoma viral oncogene homolog
LAVA	Liver acquisition with volume acquisition
MBq	Mega Becquerel
MIP	Maximum intensity projection
MR	Magnetic resonance
N/A	Not applicable
NSCLC	Non-small cell lung cancer
OP	Opposed phase
OSEM	Ordered subset expectation maximization
PET	Positron emission tomography
PET/CT	Positron emission tomography / computed tomography

PET/MR	Positron emission tomography / magnetic resonance
Propeller	Periodically rotated overlapping parallel lines with enhanced reconstruction
RF	Radiofrequency
ROC	Receiver operating characteristics
ROI	Region of interest
SD	Standard deviation
STIR	Short TI inversion recovery
SUV	Standardized uptake value
SUV_{max}	Maximum standardized uptake value
T	Tesla
TE	Time to echo
TI	Inversion time
TOF	Time of flight
TR	Time of repetition
WO	Water-only